Solid State Science and Technology, Vol. 34, No. 1 (2026) 11-18
https://doi.org/10.66514/ssst34-1-11-18

XRD and DC Conductivity Studies of CeO_2-BaO Anode Catalyst for the Robust Proton Ceramic Fuel Cell Applications

*Nurul Hazwani Yusof[1], Chung-Jen Tseng[2], Hanani Yazid[1,3], Abdul Mutalib Md Jani[3,4], Nafisah Osman[1,3]**

[1]Faculty of Applied Sciences, Universiti Teknologi MARA, 02600 Arau, Perlis, Malaysia

[2]Center for Energy Research, National Central University, No.300, Zhongda Rd., Zhongli, District, Taoyuan City 320317, Taiwan

[3]Proton Ceramic Fuel Cells Research Group, Faculty of Applied Sciences, Universiti Teknologi MARA, 40450 Shah Alam, Malaysia

[4]Faculty of Applied Sciences, Universiti Teknologi MARA, 35400 Tapah Road, Tapah, Perak, Malaysia

**Corresponding author (email: fisha@uitm.edu.my)*

(Received: 5 March 2026 / Revised: 8 May 2026 / Accepted: 14 May 2026 / Published online: 18 May 2026)

ABSTRACT

Proton ceramic fuel cells (PCFCs) demand anode materials that can operate efficiently in both hydrogen and hydrocarbon fuels. Hence, an anode reforming layer (ARL) is often introduced to enhance catalytic activity, suppress carbon deposition, and improve fuel utilization during direct hydrocarbon operation. Among various types of catalysts used as ARL, rare-earth and metal oxide-based materials are employed to ensure adequate electrical conductivity, compatibility with the anode support, and good structural stability under high temperatures. In this work, the calcined BaO and CeO_2 powders with three different ratios: 40 wt.% CeO_2–60 wt.% BaO (S1), 50 wt.% CeO_2–50 wt.% BaO (S2), and 60 wt.% CeO_2–40 wt.% BaO (S3) are dry-pressed into a 25 mm pellet, followed by solid-state sintering at T = 1050 °C. Analyses of XRD revealed that the S1, S2 and S3 (a) showed both cubic CeO_2–BaO phases with space group Fm-3m, and (b) consisting of a secondary phase of $BaCO_3$. At T = 600 °C, S2 exhibited the highest surface conductivity value (0.76 S/cm) compared to S1 (0.58 S/cm) and S3 (0.68 S/cm), making it a great potential as a high-temperature catalyst for ARL in PCFCs applications.

Keywords: Catalyst; Van Der Pauw; XRD; metal oxides; rare-earth

INTRODUCTION

Proton ceramic fuel cells (PCFCs) are solid-state electrochemical devices that convert chemical energy directly into electricity. The ability to operate at intermediate

temperature enables PCFCs to have more potential because they offer high ionic conductivity and low activation energy compared to oxygen-ion-conducting electrolyte-based solid oxide fuel cells (SOFCs) [1]. Other than that, PCFCs can operate in both hydrogen and hydrocarbon fuel, making it more preferable to be commercialized in the foreseeable future [2,3]. PCFCs' design is composed of three major components: porous electrodes (anode and cathode) and a dense electrolyte. Among the three components, the anode is very crucial to the cell's system, as the anode must simultaneously function as a catalyst for fuel oxidation and a conductor for protonic and electronic charge carriers [4,5]. The anode must also possess a material that could withstand varying redox atmospheres [6].

Currently, Ni-based material is widely being developed as an anode for PCFCs due to its excellent electronic conductivity and catalytic behavior towards hydrogen oxidation [7,8]. However, when fed with hydrocarbons such as methane (CH_4), the anode functionality becomes limited owing to the direct cleavage of C-H bonds via CH_4 reforming by the Ni-cermet anode, which leads to carbon deposition or sulfur poisoning [9,10]. Thus, these constraints will affect the cell, such as degradation of the cell performance and low catalytic activity [3]. Therefore, anode reforming layer (ARL) is being introduced and has become one of the solutions to overcome the issues regarding cell degradation. It should possess high catalytic activity, good conductivity, and thermal stability.

There are a few types of reported materials used as ARL for PCFCs, for example, yttria- stabilized zirconia (YSZ) scaffold infiltrated with Cerium oxide and platinum (CeO_2 + Pt) [11], alkaline oxides [12], rare-earth oxides [13,14] and alkaline-rare-earth oxides [3]. One of the widely adopted alkaline-rare-earth oxides is cerium-barium oxides (CeO_2-BaO) [3,8]. CeO_2 is applied as a catalyst for PCFCs due to its high oxygen storage capacity and reversible Ce^{4+}/Ce^{3+} redox behavior. In addition to it, CeO_2 can activate CH_4 and oxidize the carbon species, making it attractive to be used as a catalyst for hydrocarbon applications [15]. Meanwhile, BaO is known to possess a highly basic oxide that could mitigate the carbon formation through carbon dioxide (CO_2) adsorption and carbonate formation [8,14]. By considering the advantages of both CeO_2 and BaO, respectively, several studies can be wisely conducted to investigate the material's properties in making them suitable for the intermediate-temperature anode of PCFCs to operate in hydrocarbon fuel. However, a knowledge gap remains in correlating the structural and electrical properties of the CeO_2–BaO system at different weight ratios of both oxides. Therefore, this study aims to investigate the effect of compositional ratios on the lattice compatibility and electrical conductivity of the system.

It should be noted that this study focuses on the X-ray diffraction (XRD) for structural and DC electrical conductivities of CeO_2–BaO mixed oxides as a preliminary assessment of their potential as anode reforming layer materials. Comprehensive evaluation under practical PCFC operating conditions, particularly in hydrocarbon environments, is beyond the scope of the present work. Future works will focus on evaluating their catalytic activity, carbon deposition resistance, and long-term stability under methane-fueled PCFC operating conditions. This will enable a more comprehensive understanding of their practical performance in hydrocarbon environments.

EXPERIMENTAL DETAILS

Synthesis of Powders

To synthesize BaO powder, the barium nitrate hexahydrate ($Ba(NO_3)_2$(99% purity, Thermo Fisher Scientific)) was dissolved into 50 mL deionized water and labelled as solution A. Simultaneously, for CeO_2 powder synthesis, the cerium nitrate hexahydrate ($Ce(NO_3)_3.6H_2O$ (99.5%, purity, Thermo Fisher Scientific)) was dissolved into 50 mL deionized water and labelled as solution B. Citric acid monohydrate, CA ($C_6H_8O_7.H_2O$ (99.5% purity, Merck)) was dissolved into 50 mL deionized water and labelled as solution C. Next, solution C was accordingly poured into solutions A and B and kept stirred continuously for 2 h. The respective mixture (solution AC) and (solution BC) was then gradually heated to 80 °C until a homogeneous gel was formed and dried at 85 °C in the Venticell. The resulting powders (powder AC) and (powder BC) were ground into a fine powder and calcined using a two-step calcination. For powder AC, first at 450 °C at the rate of 2 °C/min and then at 800 °C at the same rate to form BaO. Meanwhile, for powder BC, it was first calcined at 300 °C for 2 h at the rate of 1 °C/min and then another 4 h at 450 °C at the rate of 2 °C/min to produce CeO_2.

The BaO and CeO_2 powders were mixed at 3 different ratios: 40 wt.% CeO–60 wt.% BaO (S1), 50 wt.% CeO–50 wt.% BaO (S2), and 60 wt.% CeO–40 wt.% BaO (S3) in 20 mL ethanol using a mortar and pestle. The 2.1 g of respective S1, S2 and S3 powder was weighed and placed into a 25 mm die-pressing mould and then compressed at 4.5 tones for 1.5 min. Then, the pellet was sintered (two-step sintering method) at 300 °C for 1 h with a rate of 4.5 °C/min and at 1050 °C for 3 h with a rate of 5 °C/min.

The phase and crystal structure of the samples S1, S2, and S3 were analyzed using the Shimadzu XRD-6000 in a 2θ scan range of 20° - 80° using Cu K_α radiation. The Expert HighScore Plus software was used to conduct analysis for the crystallography of the samples via the Rietveld refinement method. The electrical conductivity measurement was carried out via the Van Der Pauw (VDP) method in a hydrogen atmosphere. The DC conductivity in the temperature range from 500 °C to 800 °C was measured by using a direct current power supply (Keithley 2230-30-1, USA) and a multi-meter (Fluke 8808A, USA).

RESULTS AND DISCUSSION

XRD Patterns

Figure 1 displays the X-ray diffraction patterns of S1, S2, and S3 samples. It confirms the formation of the co-existence of BaO and CeO_2 phases across all the samples, indicating that the mixed oxide system did not form a single solid phase. They retained their individual crystalline constituents along with the secondary phase of $BaCO_3$ [16]. The prominent reflection peaks (*hkl*) corresponding to BaO were (111), (200), (220), (311), (222), (331), and (420) plane while the pronounced peak of CeO_2 can be indexed to (111), (200), (220), (311), (400), (331), and (420) plane. The noticeably lowered intensity of the $BaCO_3$ peak (~24°) compared to the BaO peak (~28°) in S2 might be due to the less availability of free reactive BaO surfaces for carbonation in the equimolar composition. This BaO residue will react with atmospheric CO_2 during the sample's processing [17,18,19]. As a result, $BaCO_3$ formation could be suppressed in S2 compared to S1 and S3. Therefore, 1 to 1 weight ratio was found as the optimized composition in promoting stronger Ce–O and Ba–O interaction to form the CeO_2-BaO system. The compositional ratio affects the phase stability and the reactivity

surface of alkaline-earth oxides due to their high affinity for carbonation, which is consistent with other reports [20,21,22].

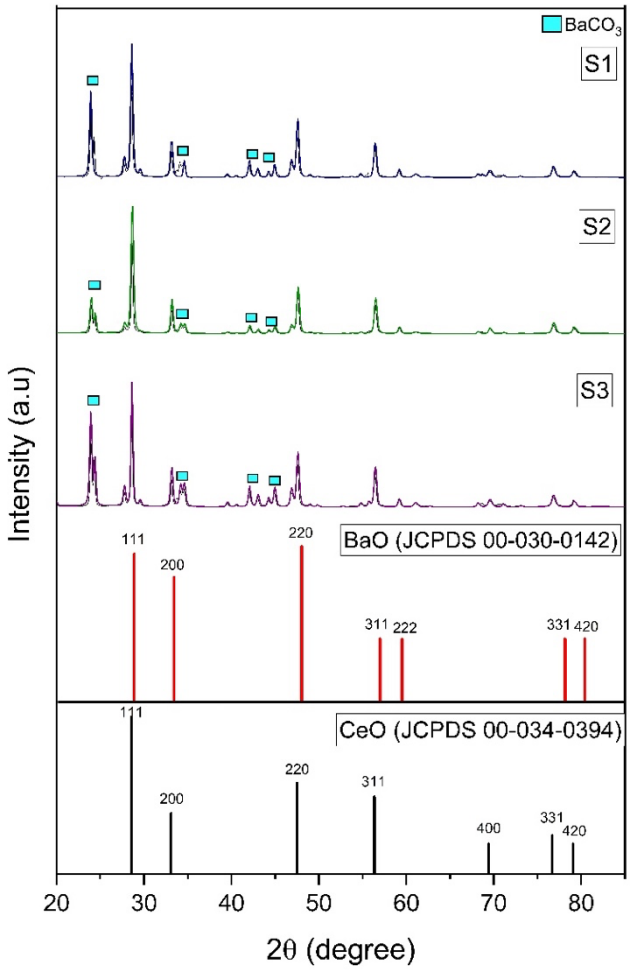

Figure 1. XRD patterns of S1, S2 and S3

All the crystallographic data obtained for S1, S2 and S3 were tabulated in Table 1, which includes the lattice parameters for both CeO_2 and BaO samples; $a = b = c$, indicating that the samples are cubic structures with a space group of Fm3m (225). The lattice parameters for CeO_2 (S1=5.4128 Å, S2=5.4124 Å and S3=5.4080 Å) and for the BaO (S1=5.4923 Å, S2=5.4098 Å, and S3=5.4054 Å). Compared to standard data for CeO_2 and BaO, respectively (Table 2), the unit cell volumes of the CeO_2 in S1=158.57 $Å^3$, S2=158.55 $Å^3$, and S3=158.17 $Å^3$ are quite matched with the reference data of 158.46 $Å^3$. Hence, it shows that the fluorite CeO_2 lattice is largely preserved in all samples' compositions, even though the slight lattice contraction can be observed in S3 due to the reduced lattice distortion in the CeO-rich composition and the increasing Ce-O bonding rigidity [23]. However, the volume of BaO in S1=165.68 $Å^3$, S2=158.33 $Å^3$ and S3=157.94 $Å^3$ was slightly bigger compared to the standard data for BaO volume (153.56 $Å^3$). The slightly enlarged BaO lattice and unit-cell volume indicate the lattice strain and defect formation arising from Ba–Ce interaction in all samples might be due to the incorporation of the Ce^{4+} ion that has a smaller ionic radius than the Ba^{2+} ion [24,25]. The S1 samples can be seen to be most affected, where excess BaO promotes lattice swelling, while progressive contraction occurs from S1 to S3 samples. Therefore, the compositional variation primarily perturbs the

BaO lattice through expansion and strain (slight peak shifting) compared to the standard BaO. Meanwhile, the CeO_2 phase remains structurally maintain highlighting the asymmetric lattice response of the CeO_2-BaO system to compositional tuning.

Table 1. Crystallography data for S1, S2 and S3 samples after Rietveld refinement

Phase parameter	S1		S2		S3	
Cell parameter (Å)	CeO_2	BaO	CeO_2	BaO	CeO_2	BaO
Lattice Parameter (Å), $a = b = c$	5.4128	5.4923	5.4124	5.4098	5.4080	5.4054
Volume (Å^3)	158.57	165.68	158.55	158.33	158.17	157.94
Alpha=Beta=Gamma	90		90		90	
Atomic Position	X		Y		Z	
Ba	0		0		0	
O	½		½		½	
Ce	0		0		0	
O	¼		¼		¼	

Table 2. Crystallographic data of standard CeO_2 and BaO samples

Sample ID	Lattice parameter (Å), $a = b = c$		Volume (Å^3)	
	CeO_2	BaO	CeO_2	BaO
JCPDS card no. 00-034-0394 CeO	5.4113		158.46	
JCPDS card no. 00-030-0142 BaO		5.3550		153.56

DC Conductivity

Figure 2 shows the result of the DC conductivity of S1, S2, and S3 samples at temperatures between 500 and 800 °C. All the samples exhibited similar trends, with conductivity decreasing as temperatures increased, indicating that all the samples displayed semiconducting behavior with negative temperature dependence. Such behaviors commonly occur for rare-earth and alkaline-earth metal oxides due to several thermodynamic and chemical degradation factors rather than intrinsic electronic transport behavior [26,27]. Based on the literature, alkaline metal oxides can react with rare-earth elements at high temperatures to form insulating compounds [17,27]. In the case of S1, S2 and S3 in the form of pellets, as they were sintered at T=1050 ºC, the formation of $BaCO_3$ and $BaCeO_3$ cannot be avoided [28,29,30]. These carbonate and cerate-based oxides are known as ionically and electrically insulating compounds [17,31,32], which may suppress the electrical conductivity of the tested samples. Another possible factor that leads to the reduction of conductivity as a function of temperature is the reduction of Ce^{4+} to Ce^{3+}, which can create electronic conductivity [17], but the tested material is designed to be a mixed ionic and electronic conductor (MIEC). This shift may alter the overall conductivity profile for the S1, S2 and S3.

Among all three samples, S2 consistently shows the highest conductivity values across all temperatures, suggesting that the 1:1 weight ratio may provide more favorable phase connectivity for charge-carrier transport. These conductivity data are consistent with the XRD results, which showed that the compositional weight ratio affects phase formation and structural characteristics. However, it should be noted that

all the above-mentioned possible reasons and claims need to be verified by the specific experimental data, and they will become our concern in future studies.

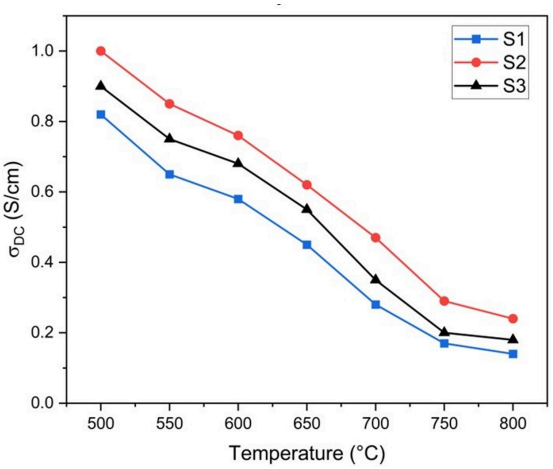

Figure 2. DC conductivity of S1, S2 and S3

CONCLUSIONS

All the prepared samples formed a cubic structure of CeO_2 and BaO, along with a secondary phase of $BaCO_3$. The composition with 50 wt.% CeO_2 and 50 wt.% BaO (S2) exhibited both lattice compatibility and the highest electrical conductivity compared to samples S1 and S3. The 1:1 weight ratio of CeO_2 to BaO appears to offer good structural integrity while enhancing electrical conductivity in a hydrogen atmosphere. These characteristics make S2 a promising high-temperature catalyst for methane reforming and electrochemical oxidation in PCFCs that operate directly on hydrocarbon fuels. Further validation is required to establish its suitability as a fully anode reforming layer material. This will enable a more comprehensive understanding of their practical performance in hydrocarbon environments.

ACKNOWLEDGEMENTS

The authors thank the Ministry of Higher Education, Malaysia, for the Fundamental Research Grant Scheme (FRGS/1/2024/STG05/UiTM/01/1) and Universiti Teknologi MARA for the Supervision Initiative Grant (GIP) (600-RMC/GIP 5/3 (007/2022)). Nurul Hazwani binti Yusof: Wrote the draft, performed visualization, collected and analyzed the data, and generated the figures. Chung-Jen Tseng: Conceptualized the research idea. Abdul Mutallib Md. Jani: Designed the research and revised the manuscript. Hanani Yazid: Supervised the research progress. Nafisah Osman: Anchored the revisions and approved the article submission.

CONFLICT OF INTEREST

The authors declare that they have no known competing financial interests or personal relationships that could have appeared to influence the work reported in this paper.

REFERENCES

[1] Liu Z, Zhou M, Chen M, Cao D, Shao J, Liu M, et al. A high-performance

intermediate-to-low temperature protonic ceramic fuel cell with in-situ exsolved nickel nanoparticles in the anode. *Ceramics International*. 2020;46(12):19952–19959.

[2] Cheng P, Lee S, Lee K, Setiawan N. ScienceDirect Carbon resistant $Ni_{1-x}Cu_x$ BCZY anode for methane-fed protonic ceramic fuel cell. *International Journal of Hydrogen Energy.* 2022;8:2–9.

[3] Shi N, Xie Y, Yang Y, Xue S, Li X, Zhu K, Huan, D, Peng R, Xia, C, Lu Y. Review of anodic reactions in hydrocarbon fueled solid oxide fuel cells and strategies to improve anode performance and stability. *Materals for Renewable and Sustainability Energy*. 2020;9(1):6.

[4] Mazlan NW, Murat MS, Tseng CJ, Hassan OH. Lattice expansion and crystallite size analyses for proton ceramic fuel cells application. *Energies.* 2022;15(22):8520.

[5] Azad AK, Abdalla AM, Afif A, Azad A, Afroze S, Idris AC, et al. Improved mechanical strength, proton conductivity and power density in an 'all-protonic' ceramic fuel cell at intermediate temperature. *Scientific Reports*. 2021;11(1):19382.

[6] Abdul L, Abdul A, Mutalib A, Jamil Z, Hidayati N, Tseng C, et al. Electrode reaction routes analyses of modified Ni-BCZY anode via distribution relaxation times : 1-D interpretation. *Materials Chemistry and Physics.* 2025;333:130353.

[7] Cho EH, Park YK, Park KY, Song D, Koo KY, Jung U, et al. Simultaneous impregnation of Ni and an additive via one-step melt-infiltration: Effect of alkaline-earth metal (Ca, Mg, Sr, and Ba) addition on $Ni/\gamma\text{-}Al_2O_3$ for CO_2 methanation. *Chemical Engineering Journal*. 2022;428:131393.

[8] Wei K, Wang X, Budiman RA, Kang J, Lin B, Zhou F, et al. Progress in Ni-based anode materials for direct hydrocarbon solid oxide fuel cells. *Journal of Materials Science.* 2018;53(12):8747–65.

[9] Xu Q, Guo Z, Xia L, He Q, Li Z, Temitope I, et al. A comprehensive review of solid oxide fuel cells operating on various promising alternative fuels. *Energy Conversion Management.* 2022;253:115175.

[10] Dai M, Tong Y, He W, Jiang S, Sun Z, Sun W, et al. Tuning ceramic-metal wettability of nickel cermets for efficient and durable hydrogen oxidation and evolution in protonic ceramic cells. *ACS Applied Materials & Interfaces*. 2025; 17(26):37879–37888.

[11] Park J, Hao NH. Direct ethanol-fueled protonic ceramic fuel cell with reforming layer operating at low temperature. *International Journal of Hydrogen Energy*. 2023;48(50):19207–19216.

[12] Qiu P, Sun S, Yang X, Chen F, Xiong C, Jia L, et al. A review on anode on-cell catalyst reforming layer for direct methane solid oxide fuel cells. *International Journal of Hydrogen Energy.* 2021;46(49):25208–25224.

[13] Naikoo GA, Arshad F, Hassan IU, Tabook MA, Pedram MZ, Mustaqeem M, et al. Thermocatalytic hydrogen production through decomposition of methane-a review. *Frontiers in Chemistry*. 2021;9:736801.

[14] Liu F, Duan C. Direct-hydrocarbon proton-conducting solid oxide fuel cells. *Sustainability.* 2021;13:4736.

[15] da Fonseca RO, Rabelo-Neto RC, Simões RCC, Mattos L V., Noronha FB. Pt supported on doped $CeO2/Al_2O_3$ as catalyst for dry reforming of methane. *International Journal of Hydrogen Energy*. 2020;45(8):5182–5191.

[16] Lacz A. Effect of microstructure on chemical stability and electrical properties of $BaCe_{0.9}Y_{0.1}O_{3-\delta}$. *Ionics*. 2016;22:1405–1414.

[17] Li K, Li H, Wei S, Liu Y, Li Y, Zhang R, et al. High performance $BaCO_3CeO_2$ composite catalyst for solvent-free selective oxidation of cyclohexane with molecular oxygen. *Molecular Catalysis*. 2023;535:112851.
[18] Wu Z, Jiang L, Dong Q, Gao Q, Cai J, Cheng X. Effect and mechanism of rare Earth and alkaline Earth metals on the high-temperature stability of activated alumina. *Frontiers in Materials.* 2023;10:1103590.
[19] Abd AN, Abdulmahdi N, Al J, Abad WK, Abd AN. Synthesis of barium oxide nanoparticles by simple chemical method and its applications as a solar. ACE *Journal of Advance Research in Chemical Sciences.* 2023;3(1):10-17.
[20] Karslıoğlu O, Trotochaud L, Zegkinoglou I, Bluhm H. X-ray spectroscopic characterization of BaO, $Ba(OH)_2$, $BaCO_3$, and $Ba(NO_3)_2$. *Journal of Electron Spectroscopy and Related Phenomenon.* 2018;225:55-61.
[21] Guo Y, Ran R, Shao Z, Liu S. Effect of Ba nonstoichiometry on the phase structure, sintering, electrical conductivity and phase stability of $Ba_{1\pm x}Ce_{0.4}Zr_{0.4}Y_{0.2}O_{3-\delta}$ ($0\leq x\leq 0.20$) proton conductors. *International Journal of Hydrogen Energy.* 2011;36(14):8450–60.
[22] Zheng Y, He S, Ge L, Zhou M, Chen H, Guo L. Effect of Sr on Sm-doped ceria electrolyte. *International Journal of Hydrogen Energy*. 2011;36(8):5128–35.
[23] Kimmel G, Sahartov A, Sadia Y, Porat Z, Zabicky J, Dvir E. Non-monotonic lattice parameters variation with crystal size in nanocrystalline CeO_2. *Journal of Materials Research Technology*. 2021;12:87-99.
[24] Tanwar K, Gyan DS, Gupta P, Pandey S, Parkash O, Kumar D. Investigation of crystal structure, microstructure and low temperature magnetic behavior of Ce^{4+} and Zn^{2+} co-doped barium hexaferrites ($BaFe_{12}O_{19}$). *RSC Adv.* 2018;8:19600.
[25] Pham CN, Trinh Q Van, Thai D Van, Dao NN, Nguyen BQ, Doan DT, et al. Synthesis of CeO_2-Fe_2O_3 mixed oxides for low-temperature carbon monoxide oxidation. *Adsorption Science & Technology.* 2022;2022:5945169.
[26] Hota OP, Mohanty P, Mahapatra R. Future research direction on rare-earth and alkaline-earth metal-doped $LaMnO_3$ perovskites. *Brazilian Journal of Physics* 2025;55:272.
[27] Halizan, M.Z.; Mohamed, Z. Dielectric, AC conductivity, and DC conductivity behaviours of Sr_2CaTeO_6 double perovskite. *Materials* 2022;15:4363.
[28] Osman N, Mazlan NW, Hassan OH, Zulkifli WZW, Mohamed Z. Phase analysis of cerate and zirconate ceramics powder prepared by supercritical ethanol using high temperature-high pressure batch wise reactor system. *Solid State Phenomena.* 2020;307:171–175.
[29] Asyikin N, Nafisah M, Abdul O, Jani M. Role of ionic and nonionic surfactant on the phase formation and morphology of $Ba(Ce,Zr)O_3$ solid solution. *Journal of Sol-Gel Science and Technology*. 2016;78(1):50–59.
[30] Mazlan NW, Osman N, Hassan OH. Thermal expansion and lattice parameter of solid electrolyte based on cerate-zirconate ceramics. *AIP Conference Proceedings*. 2018;2031:020014.
[31] Osman N, Mazlan NA, Affandi NSM, Mazlan NW, Md Jani AM. Optimization of electrolyte performance by tailoring the structure and morphology of $Ba(Ce,Zr)O_3$ ceramics with different types of surfactants. *Ceramics International*. 2020;46(17):27401-27409
[32] Katahira K, Kohchi Y, Shimura T, Iwahara H. Protonic conduction in Zr-substituted $BaCeO_3$. *Solid State Ionics.* 2000;138(1–2):91–98.